Modelling and Validation of Rotor-Active Magnetic Bearing System Considering Interface Contact

Yang Zhou[1], Jin Zhou[1(✉)], Jarir Mahfoud[2], Yue Zhang[1], and Yuanping Xu[1]

[1] College of Mechanical and Electrical Engineering,
Nanjing University of Aeronautics and Astronautics, Nanjing 210016, China
{zhouyang0216,zhj,zhangyue08,ypxu}@nuaa.edu.cn
[2] University of Lyon, Lyon, France

Abstract. Rotor-active magnetic bearing (rotor-AMB) system is increasingly applied in rotating machinery such as blowers, compressors, vacuum pumps, etc. However, due to the coupling of interface contact (such as bolt-joint surface and cylindrical-joint surface) formed by impeller assembly and AMB supporting, the rotor will vibrate at a modal frequency once levitated, which causes system instability and equipment breakdown. Therefore, it is essential to reveal the principle of this vibration. In rotor modelling, interface contact is equivalent to an additional stiffness matrix based on a massless spring unit. The value of the matrix is obtained by energy law. Subsequently, interface contact's influence is considered an internal disturbance in the rotor-AMB system. This modelling method is validated by different test rigs. Through rotor response and stability analysis of different test rigs, it is found that rotor modal resonance mode depends on contact interface parameters (such as bolt pre-tightening force). Based on these results, stability analysis is carried out to study the general relationship between system stability and contact interface parameters, which will further reveal the vibration mechanism and guide the following maglev machine structural design to avoid this vibration.

Keywords: Interface Contact · Contact stiffness · Active Magnetic Bearing · Mechatronics Modelling · Modal Resonance

1 Introduction

Active magnetic bearings (AMBs) have been widely used in centrifugal gas compressors and other high-speed rotating machinery applications [1]. AMBs do not need lubrication, and their non-contact environment significantly reduces friction, making the system efficient. Another attractive advantage of AMBs is that the electromagnetic force is controlled and changed actively through AMBs, making the rotor work stably at high speed. As an indispensable part of rotating machinery, the impeller is also needed in the magnetic levitation compressor. However, rotor assembled with the impeller constantly vibrates intensely in high frequency during levitation which significantly influences

F. Chu and Z. Qin (Eds.): IFToMM 2023, MMS 139, pp. 374–390, 2024.
https://doi.org/10.1007/978-3-031-40455-9_31

the system's stability. This phenomenon is successively found in magnetic levitation machines like blowers, compressors, vacuum pumps, etc. This problem is caused by the coupling of the influence of assembly interface contact and complex electromechanical characteristics of AMB system. Few types of researches on these two aspects have been carried out.

On the aspect of the influence of assembly interface contact, Tan [2] modeled the shrink-fit interface of the rotor as the internal damping force and analyzed it's influence on the system stability by decomposing the asymmetric stiffness component from the system equations. Liu [3] adopted the spring unit to simulate the interface contact formed by rod-fastened structure and analyzed the instability factor caused by the odds of the pre-tightening force of the rod. Liao et al. [4] and Liu et al. [5] adopted thin-layer elements to simulate the complicated interface contact based on the finite element method. The interface contact significantly influences the system stability from the researches above. However, researches are all based on the excitation of rotation, and a complex model of interface contact is not suitable in AMB system.

On the other aspect of the complicated electromechanical characteristics of the AMB system, Yannick Paul [6] mentioned that the bad connection between the rotor and the impeller may cause high-frequency vibration during levitation. Wei [7] equaled the influence of shrinkage fit in AMB-rotor to a disturbance in the direction of rotation considering that the rotor is rigid. Simon [8, 9] analyzed the influence of material internal damping in the direction of translation based on modelling of a flexible rotor and design a robust controller based on the model above. The interface contact can only be equivalent to disturbance rather than the influence on system stability due to the limitation of rotor modelling. However, the modelling of electromechanical characteristics of the AMB system can be combined with the modelling of interface contact. The researches above lack the study of the influence of interface contact on internal system and fail to obtain the clear relationship between disturbance and property of contact interface such as magnitude of interference.

In this paper, we present the modelling of the magnetic bearing-rotor system considering interface contact based on the modelling of interface contact and modelling of the magnetic bearing-rotor system. The spring unit with specific contact stiffness is used to simulate the interface contact of the rotor and impeller in the form of an additional stiffness matrix added to the system dynamics equation. The dynamic characteristic of magnetic bearing-rotor system considering interface contact is obtained by comparing the response and frequency of vibration of different pre-tightening torque based on simulation and experiment results.

This paper proceeds as follows. Section 2 presents the modelling of magnetic bearing-rotor system and interface contact. In Sect. 3, the numerical simulation and the experimental validation are described. Section 4 presents the stability analysis. Section 5 concludes the paper.

2 Modelling of the Rotor-AMBs System Considering Interface Contact

2.1 Modelling of the Rotor-AMBs System

As shown in Fig. 1(a), the rotor-AMBs system is divided into three parts: the rotor model, the model of the electronic control system, and the model of interface contact. The structure of a radial magnetic bearing is shown in Fig. 1(b). A sensor measures the displacement of the rotor from its reference position, a microprocessor as a controller derives a control signal from the measurement, a power amplifier transforms this control signal into a control current, and the control current generates a magnetic field in the actuating magnets, resulting in magnetic forces in such a way that the rotor remains in its hovering position.

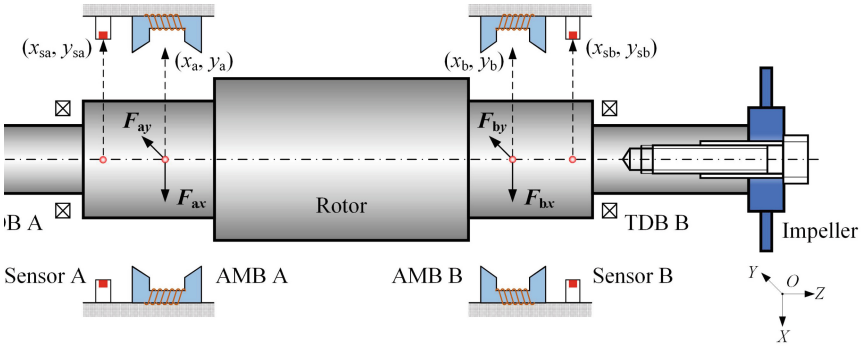

(a) Structure of the rotor-AMBs system

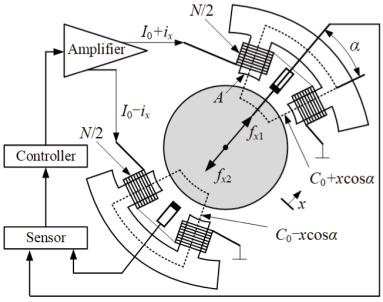

(b) Structure of the radial magnetic bearing

Fig. 1. Schematic diagram of rotor-AMB mechatronic system considering interface contact.

The theory of the Bernoulli-Euler beam is applied to the finite element modelling of the rotor. The equation of the rotor-AMB mechatronic model takes the following form:

$$M_R\ddot{q} + (C_R + \omega G_R)\dot{q} + K_R q = T_a^T f_a + T_u^T f_u \tag{1}$$

where M_R, C_R, G_R, and K_R respectively represent the mass matrix, the damping matrix, the gyroscopic matrix, and the stiffness matrix of the rotor, ω is the rotation frequency, f_a

$= [F_{ax}\ F_{ay}\ F_{bx}\ F_{by}]$, represents the electromagnetic force vector in the x and y directions generated by the AMBs A and B, T_a is the transfer matrix of the AMB nodes, and f_u represents the unbalanced force vector in the x, y directions, T_u is the transfer matrix of the unbalance mass nodes. q are system displacements and angles vector under the Cardan description.

The radial magnetic force is modeled as a generalized external force. Near the equilibrium point, the magnetic force can be approximated as Eq. (2)

$$f_a = \left[F_{\mathrm{AMB,A}x}\ F_{\mathrm{AMB,Ay}}\ F_{\mathrm{AMB,B}x}\ F_{\mathrm{AMB,By}} \right]^T = k_x q_a + k_i i_a \tag{2}$$

where k_x and k_i are displacement stiffness and current stiffness, respectively. q_a and i_a are the radial displacements of AMBs nodes and control currents.

The relationship between control currents and the radial rotor displacement q_s detected by sensors is given as Eq. (3)

$$i_a = S(s)A(s)C(s)q_s = k_s \cdot \frac{k_a(2\pi f_z)}{s+(2\pi f_z)} \cdot \left(K_P + \frac{K_I}{T_I s + 1} + \frac{K_D s}{T_D s + 1} \right) q_s \tag{3}$$

where $S(s)$, $A(s)$, and $C(s)$ is the transfer function of the sensor, amplifier, and the controller, respectively. k_s is the gain of the sensor. k_a is the gain of the power amplifier, and f_z is the cut-off frequency. K_P, K_I and K_D respectively represent the proportional gain, the integral gain, the derivative gain. T_D is the derivative time constant.

2.2 Modelling of Interface Contact

In the modelling of interface contact, the interface contact between the disk and the rotor is equivalent to spring units uniformly distributed over the contact interface, as shown in Fig. 2(a). The spring unit connects any point A (x_A, y_A, z_A) on the rotor contact interface and its corresponding point B (x_B, y_b, z_B) on the disk contact interface. The stiffness of the massless spring unit is referred to as contact stiffness. The contact stiffness can be subdivided into the normal contact stiffness k_f and the tangential contact stiffness k_q. The directions of k_f and k_q are perpendicular and parallel to the contact interface, respectively. There is relative deformation between the contact interfaces when the rotor vibrates. The energy generated by the spring deformation is calculated to study the influence of interface contact.

As shown in Fig. 2(b), floating coordinates $o_i x_3 y_3 z_3$ and $o_j x_3 y_3 z_3$ are established by taking the contact interface centers i and j as the coordinate origin and coordinate transformation in order to obtain the relative deformations of the spring unit in x, y, z directions. The generalized coordinates of centers i and j are (x_i,y_i,α_i,β_i,z_i,ωt) and (x_j,y_j,α_j,β_j,z_j,ωt) in the absolute coordinate system $oxyz$, where x_i, y_i, and z_i (x_j, y_j, and z_j) are the translations of i (j) in the x, y and z directions and α_i, β_i, and ωt (α_j, β_j, and ωt) are the rotations of i (j) around the x, y and z axis, $x_3 y_3$ plane coincides with the contact interface and the orientation of z_3 is perpendicular to the contact surface. In a floating coordinate system, the coordinates of points A and B can be determined by the polar coordinates (r,θ), where r represents the distance between point A and center i or the distance between point B and center j, θ represents the angle between line Ai, Bj and x_3 axis, counterclockwise.

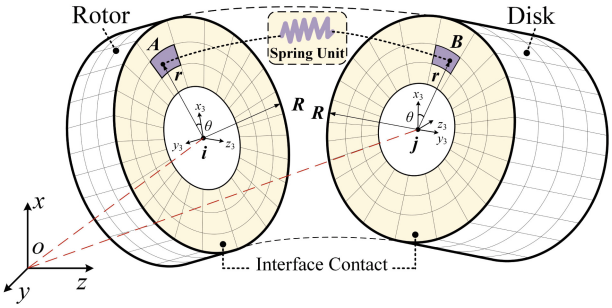

(a) Dynamic model of interface contact

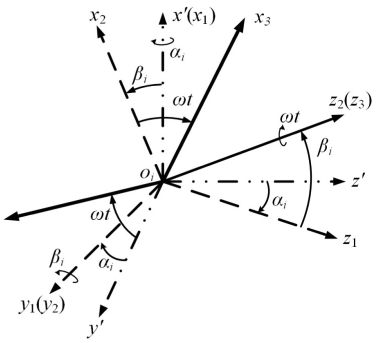

(b) Diagram of coordinate transformation

Fig. 2. Modelling of interface contact.

The total energy generated by the spring unit is obtained by summing up the unit spring energy Δu as Eq. (4).

$$\begin{aligned} u &= \iint_{\mathrm{A}} \frac{1}{2}\left(k_q \Delta x^2 + k_q \Delta y^2 + k_f \Delta z^2\right) d\mathrm{A} \\ &= 0.5k_q \iint_{\mathrm{A}} d\mathrm{A}\left[\left(x_j - x_i\right)^2 + \left(y_j - y_i\right)^2\right] \\ +0.5k_f &\iint_{\mathrm{A}} y^2 d\mathrm{A}\left(\alpha_j - \alpha_i\right)^2 + 0.5k_f \iint_{\mathrm{A}} x^2 d\mathrm{A}\left(\beta_j - \beta_i\right)^2 \end{aligned} \tag{4}$$

where $\Delta x = x_{\mathrm{B}}\text{-}x_{\mathrm{A}}$, $\Delta y = y_{\mathrm{B}}\text{-}y_{\mathrm{A}}$, $\Delta z = z_{\mathrm{B}}\text{-}z_{\mathrm{A}}$, R is the radius of the contact interface, R_b is the radius of the bolt hole. The total energy of the spring unit can be expressed as the elastic potential energy Eq. (5).

$$\begin{aligned} u &= \frac{1}{2}\left[\, q_i \; q_j \,\right] K_e \left[\, q_i \; q_j \,\right]^T \\ K_e &= \begin{bmatrix} diag\left(k_p, k_p, k_c, k_c\right) & -diag\left(k_p, k_p, k_c, k_c\right) \\ -diag\left(k_p, k_p, k_c, k_c\right) & diag\left(k_p, k_p, k_c, k_c\right) \end{bmatrix} \\ k_p &= k_q \pi \left(R^2 - R_b^2\right), \quad k_c = 0.25 k_f \pi \left(R^4 - R_b^4\right) \end{aligned} \tag{5}$$

where K_e is the additional stiffness matrix generated by interface contact.

Based on the Lagrange equation, the force generated by the interface contact is expressed Eq. (6).

$$F_c = K_e \left[q_i \; q_j \right]^{\mathrm{T}} = K_e T_c q \tag{6}$$

The disturbance introduced by the disk assembly arises from the slight fluctuation between the contact interfaces during the suspension. To sum up, the closed-loop model of the rotor-AMBs system considering interface contact can be expressed as Eq. (7).

$$M_R \ddot{q} + (C_R + \omega G_R)\dot{q} + K_R q = k_x T_a^T T_a q + k_i T_a^T i_a + T_c^T K_e T_c q \tag{7}$$

where T_c is the transfer matrix of the interface contact nodes m and n.

The disturbance F_c acts on the system as the generalized force and its value is related to the rotor's vibration amplitude. The response of the closed-loop system is influenced by the disturbance F_c. The disturbance will excite the unstable modal vibration. When the modal frequency is within the control bandwidth of the magnetic bearing, the system is able to control the disturbance. But when the modal frequency is out of the control bandwidth of the magnetic bearing, the control effect will decrease as the disturbance increase (Fig. 3).

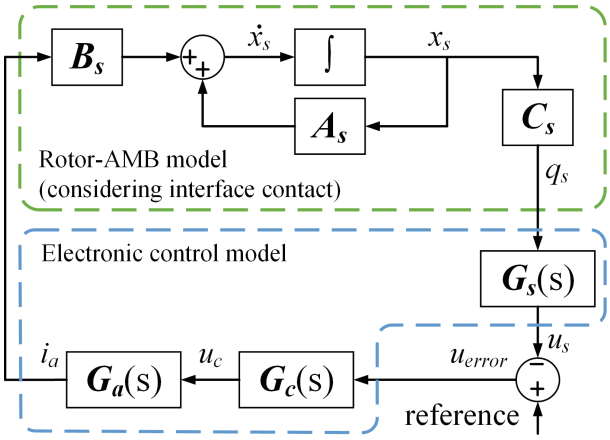

Fig. 3. Diagram of the closed-loop mathematical model.

3 Numerical Simulation and Experiment Validation of Different Magnetically Suspended Rotors

In this section, two different magnetically suspended rotors are modelled and the influences of interface contact are investigated. The numerical simulation results are verified by experiments.

3.1 Magnetic Levitation Blower

The structure of the magnetic levitation blower is shown in Fig. 4. It can be seen that the impeller is connected to the rotor by bolted joint, which forms the interface contact between the rotor and the impeller.

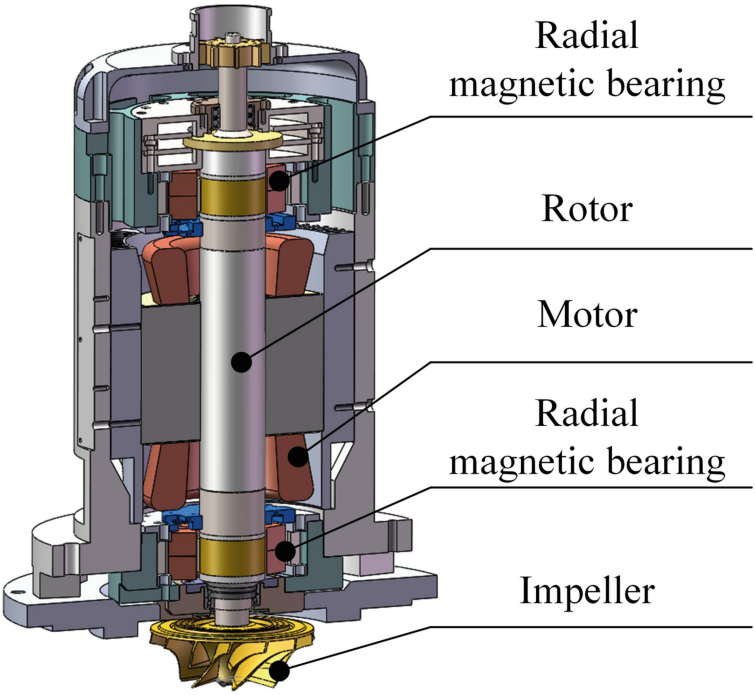

Fig. 4. Typical structure of the magnetic levitation blower.

Based on the modelling method, the mechatronic model of the magnetic levitation blower is established. The rotor is modeled with 74 beam elements for a total mesh of 296 DOF for the lateral analysis (see Fig. 5). Based on the modal test, the experimental and theoretical bending mode frequencies of the rotor with bolted joint are shown in Table. 1.

The simulation of the mechatronic model considering interface contact is shown in Fig. 6(a), (b). The system is unstable and the rotor vibrates at the second bending mode when the disturbance F_c caused by interface contact acts on the system. The vibration of the second bending mode is excited by interface contact, the displacements of the rotor are increased rapidly.

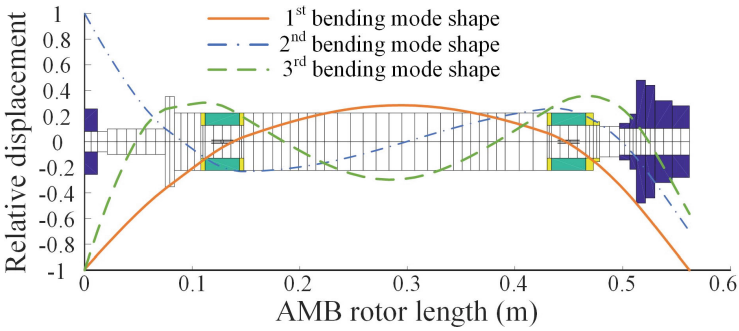

Fig. 5. Theoretic mode shapes of the free-free rotor (magnetic levitation blower)

Table. 1. The bending mode frequencies of the rotor in magnetic levitation blower.

Order	Experimental frequency (Hz)	Theoretical frequency (Hz)
1st mode	735.12	730.05
2nd mode	1245.66	1234.7
3rd mode	1892.25	2057.3

Figure 7(a), (b) presents the experimental results when the disk is connected to the rotor by bolt fastening. The rotor displacement in the A_x direction is in a similar tendency to simulation results. From spectral analysis (fast Fourier transform, FFT), the second bending mode frequency exists when interface contact exists in the rotor. The influences of interface contact and order of vibration mode agree with the simulation, which verifies the model's accuracy.

The influence of the normal contact stiffness on the rotor displacement is shown in Fig. 8. Varying the value of the normal contact stiffness from 6×10^{13} N/m^3 to 10×10^{13} N/m^3, as shown in Fig. 8(a), time domain response shows that, as k_f increases, the amplitude of the response increases and instability becomes more apparent. In the frequency domain shown in Fig. 8(b), the second bending mode frequency vibration increases as the normal contact stiffness increases.

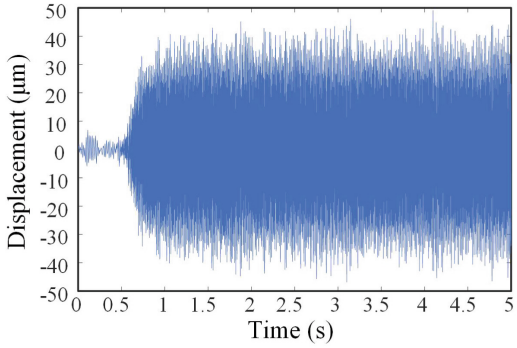

(a) Rotor time-domain response

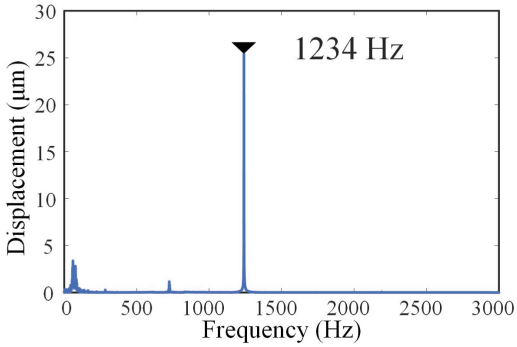

(b) Rotor frequency-domain response

Fig. 6. Rotor response in simulation (magnetic levitation blower).

3.2 Magnetic Levitation Motor

The structure of the magnetic levitation motor is shown in Fig. 9. The coupling is connected to the rotor by bolted joint, which forms the interface contact between the rotor and the coupling.

The mechatronic model of the magnetic levitation blower is established based on the modeling method. The rotor is modeled with 76 beam elements for a total mesh of 304 DOF for the lateral analysis (see Fig. 10). Based on the modal test, the experimental and theoretical bending mode frequencies of the rotor with bolted joint are shown in Table. 2.

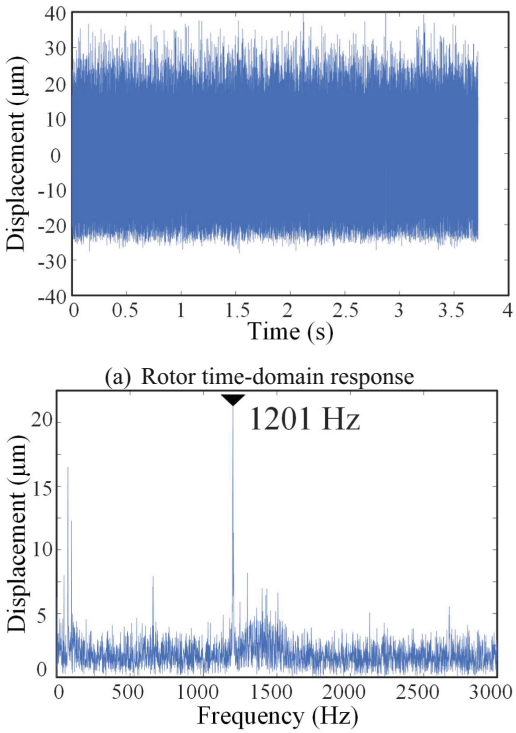

(a) Rotor time-domain response

(b) Rotor frequency-domain response

Fig. 7. Rotor response in experiment (magnetic levitation blower).

The simulation of the mechatronic model considering interface contact is shown in Fig. 11(a), (b). The system is unstable and the rotor vibrates at the first bending mode when the disturbance F_c caused by interface contact acts on the system. The vibration of the first bending mode is excited by interface contact, the displacements of the rotor are increased rapidly.

Figure 12(a), (b) presents the experimental results when the disk is connected to the rotor by bolt fastening. The rotor displacement in the A_x direction is in a similar trend as simulation results. From spectral analysis, there is the first bending mode frequency when interface contact exists in the rotor. The influences of interface contact and order of vibration mode agree with the simulation, which verifies the model's accuracy.

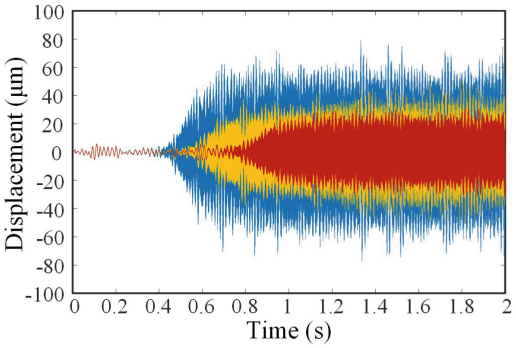

(a) Comparison of rotor time-domain responses (different normal contact stiffness)

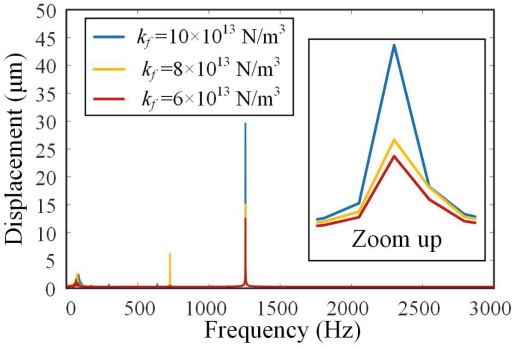

(b) Comparison of rotor frequency-domain responses (different normal contact stiffness)

Fig. 8. Comparison of dynamic responses in magnetic levitation blower (different normal contact stiffness).

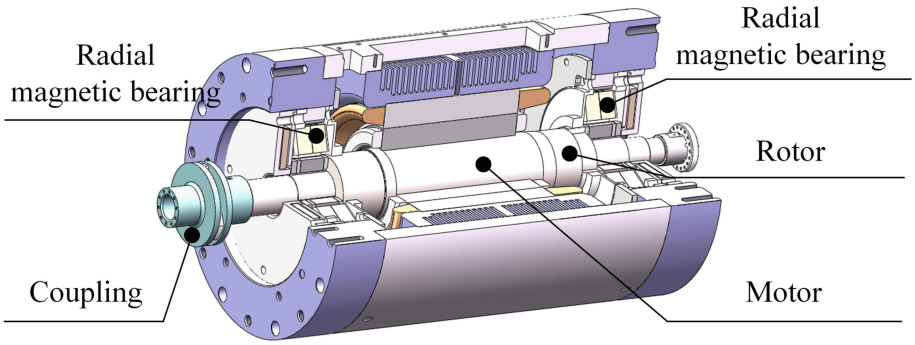

Fig. 9. Typical structure of the magnetic levitation motor.

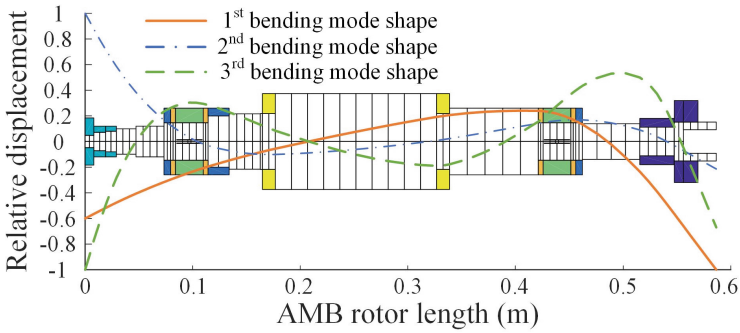

Fig. 10. Theoretic mode shapes of the free-free rotor (magnetic levitation motor).

Table. 2. The bending mode frequencies of the rotor in magnetic levitation motor.

Order	Experimental frequency (Hz)	Theoretical frequency (Hz)
1^{st} mode	720.87	705.9
2^{nd} mode	1503.89	1511.13

The influence of the normal contact stiffness on the rotor displacement is shown in Fig. 13. Varying the value of the normal contact stiffness from 6×10^{13} N/m^3 to10×10^{13} N/m^3, as shown in Fig. 13(a), time domain response shows that, as k_f increases, the amplitude of the response increases and instability becomes more obvious. In the frequency domain shown in Fig. 13(b), the first bending mode frequency vibration increases as the normal contact stiffness increases.

4 System Stability Analysis

For linear time-invariant (LTI) systems, root locus analysis is applied in this study. The stability analysis of the magnetic levitation blower system and the magnetic levitation motor system are depicted in Fig. 14, respectively.

From the root locus of magnetic levitation blower system, varying the value of the normal contact stiffness from 1×10^{13} N/m to 10×10^{13} N/m, the root locus of the closed-loop system is shown in Fig. 14(a). As k_f increases, the characteristic roots of the third bending modes move towards the negative direction of the real axis and the real parts of these roots are all negative. On the contrary, as k_f increases, the characteristic roots of first and second bending modes move towards the positive direction of the real axis and the real parts of the second bending mode roots turn from negative to positive. As the real part of a system's characteristic root becomes positive, the system becomes unstable. As k_f increases, the real parts of the second bending mode roots become positive, which leads to high-frequency vibration. Because the first bending mode roots also move towards the positive direction, the vibration of the first bending mode is also excited, as shown in Fig. 6 and Fig. 7. But these roots do not cross the imaginary axis,

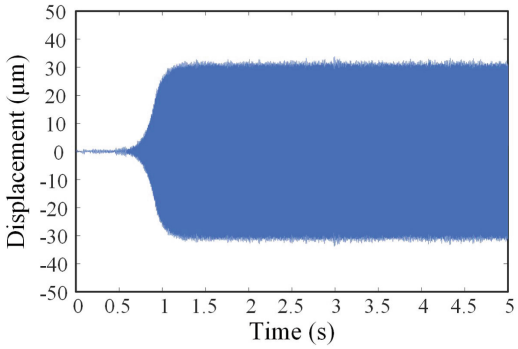

(a) Rotor time-domain response

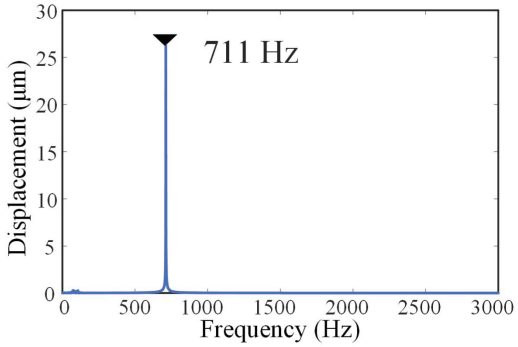

(b) Rotor frequency-domain response

Fig. 11. Rotor response in simulation (magnetic levitation motor).

the vibration amplitude of the first bending mode is smaller than the vibration amplitude of the second bending mode.

From the root locus of the magnetic levitation motor system, varying the value of the normal contact stiffness from 1×10^{13} N/m to 10×10^{13} N/m, the root locus of the closed-loop system is shown in Fig. 14(b). As k_f increases, the characteristic roots of the second and third bending modes move towards the negative direction of the real axis and the real parts of these roots are all negative. On the contrary, as k_f increases, the characteristic roots of first bending modes move towards the positive direction of the real axis and the real parts of the first bending mode roots turn from negative to positive. As the real part of a system's characteristic root becomes positive, the system becomes unstable. As k_f increases, the real parts of the first bending mode roots become positive, which leads to high-frequency vibration.

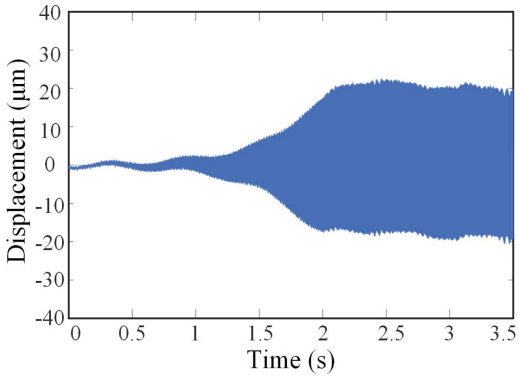

(a) Rotor time-domain response

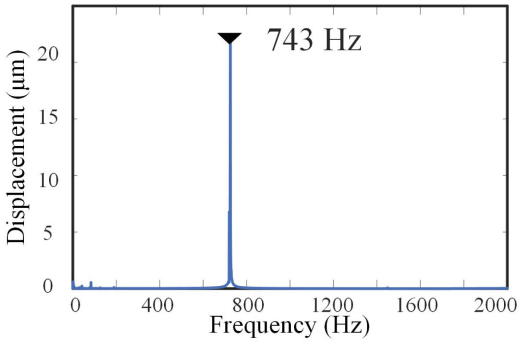

(b) Rotor frequency-domain response

Fig. 12. Rotor response in experiment (magnetic levitation motor).

The contact stiffness is related to the pre-tightening torque [10], the normal and tangential contact stiffness increase as the increase of the pre-tightening torque. To sum up, when the pre-tightening torque of the bolted joint increases, the contact stiffness increases, which will make the roots of the unstable mode move towards the positive direction and cross the imaginary axis. As a result, unstable modal vibration will be caused.

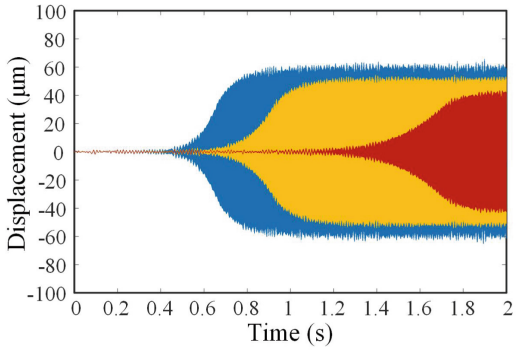

(a) Comparison of rotor time-domain responses (different normal contact stiffness)

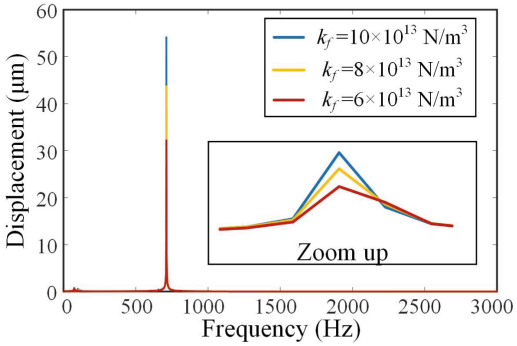

(b) Comparison of rotor frequency-domain responses (different normal contact stiffness)

Fig. 13. Comparison of dynamic responses in magnetic levitation motor (different normal contact stiffness).

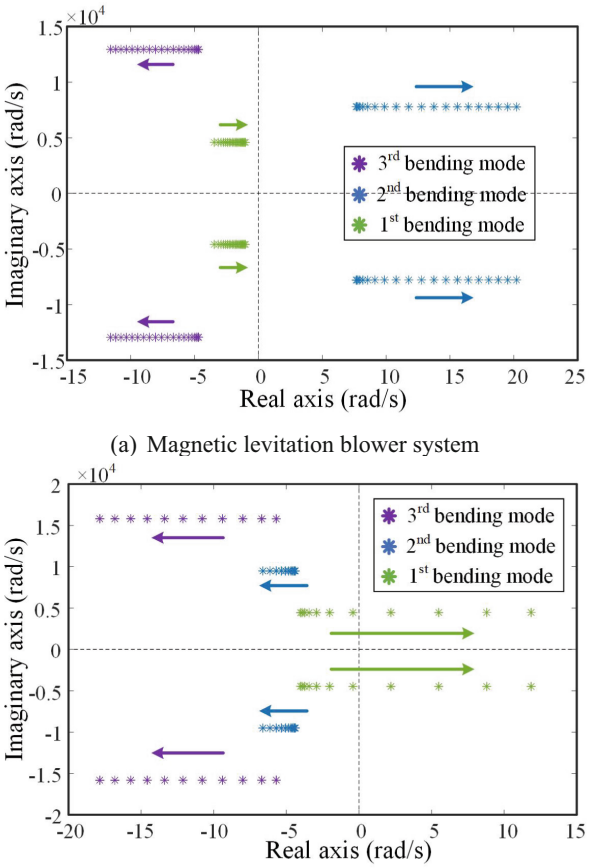

(a) Magnetic levitation blower system

(b) Magnetic levitation motor system

Fig. 14. Root locus of the closed-loop system.

5 Conclusion

This paper studies the modal vibration caused by interface contact in rotor-AMB systems when the rotor is levitated without rotating by establishing the mechatronic rotor-AMB model considering the interface contact. The mechanism of this high-frequency vibration and the contributing influences of the pre-tightening torque are revealed by combining the results of dynamic analysis and experimental validation.

There is a slight fluctuation of the rotor when being levitated by AMBs because rotor-AMB systems are active systems. Therefore, there are multivariant slight vibrations in the contact interfaces formed by the rotor and the disk. Such vibrations are amplified into an internal disturbance of the system by the effect of the contact stiffness matrix of the contact interface. The internal disturbance caused by the interface contact and the energy input from the AMB supporting increases as the pre-tightening torque increases. From the results of root locus analysis, as the internal disturbance increases, the roots of

the unstable modes move towards the positive direction of the real axis and the system stability weakens. When the real part of a root turns from negative to positive, the system turns from stable to unstable, and modal vibration is excited.

References

1. Schweitzer, G., Maslen, E.H.: Magnetic bearings. Springer, Berlin (2009)
2. Tan, D., Chen, J., Liao, M., Wang, S.: Instability caused by cylindrical surface fit in rotor system. Mechan. Sci. Technol. Aeros. Eng. **33**, 1786–1790 (2014)
3. Liu, Y., Liu, H., Yi, J., Jing, M.: Investigation on the stability and bifurcation of a rod-fastening rotor bearing system. J. Vib. Control **21**, 2866–2880 (2014)
4. Liao, H., Zang, C., et al.: Dynamic modelling and updating for contact interface of rod fastening rotor based on thin-layer element. J. Aeros. Power **34**(9), 1927–1935 (2019)
5. Liu, Y., Liu, H.., et al.: Image method for measuring normal interfacial stiffness. J. Eng. Tribolo. **0**(0), 1–14 (2016)
6. Paul, Y., Smithanik, J.: New API 617 standards applied to magnetic bearings turbo-expanders. Chinese Journal of Turbomachinery **058**(005), 6–18 (2016)
7. Wei, T., Fang, J.: Self-excited vibration depression of high-speed rotor in magnetically suspended control moment gyroscope. Journal of Astronautics (02), 291–296 (2006)
8. András S., Flowers, G.: Suppression of internal damping-induced instability using adaptive techniques. In: ASME International Design Engineering Technical Conferences & Computers & Information in Engineering Conference, Las Vegas (2007)
9. András, S., Flowers, G.T.: Adaptive disturbance rejection and stabilization for rotor systems with internal damping. In: ASME International Design Engineering Technical Conferences & Computers & Information in Engineering Conference. San Diego (2009)
10. Shi, W., Zhang, Z.: Contact characteristic parameters modelling for the assembled structure with bolted joints, Tribology International 165 (2022)